Journal of chemical & engineering data

Article

pubs.acs.org/jced

Enhancing Liquid-Phase Olefin−Paraffin Separations Using Novel Silver-Based Ionic Liquids

Yu Wang,[†] Weiye Hao,[†] Johan Jacquemin,[†] Peter Goodrich,[†] Mert Atilhan,[‡] Majeda Khraisheh,*[,‡] David Rooney,[†] and Jillian Thompson[†]

[†]The QUILL Research Centre, School of Chemistry and Chemical Engineering, Queen's University, Stranmillis Road, Belfast, Northern Ireland BT9 5AG, United Kingdom

[‡]Department of Chemical Engineering, Qatar University, PO Box 2713, Doha, Qatar

Supporting Information

ABSTRACT: This paper describes the extraction of C5−C8 linear α-olefins from olefin/paraffin mixtures of the same carbon number using silver(I)/*N*,*N*-dimethylbenzamide bis(trifluoromethylsulfonyl)imide ($[Ag(DMBA)_2][Tf_2N]$) or silver(I)/propylamine bis(trifluoromethylsulfonyl)imide ($[Ag(PrNH_2)_2][Tf_2N]$) as the extracting agent. The separation performance of the system increased with increasing chain length. $[Ag(DMBA)_2][Tf_2N]$ appeared to outperform $[Ag(PrNH_2)_2][Tf_2N]$ in terms of both selectivity and distribution coefficient. The $[Ag(DMBA)_2][Tf_2N]$ system was successfully modeled using the universal quasi-chemical activity coefficient (UNIQUAC) model. These results support the potential future development of amine/amide-based ligands for producing soluble silver complexes useful for the separation of olefins from paraffins.

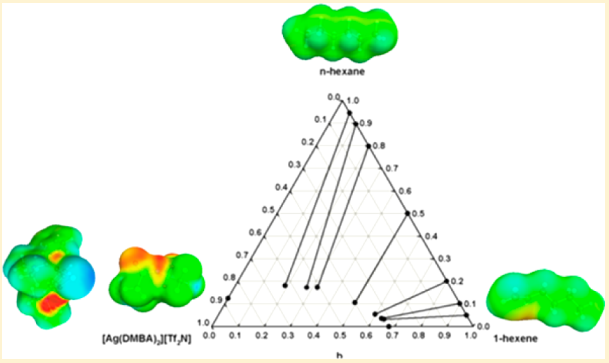

1. INTRODUCTION

The separation of unsaturated hydrocarbons (olefins) from saturated hydrocarbon (paraffin) streams is of great importance industrially. Olefins such as ethylene are major building blocks in the production of polymers and are widely produced by cracking feedstocks such as naphtha or ethane. The product streams from these cracking processes often contain alkanes and alkenes with the same carbon number (e.g., the C2 compounds ethane and ethylene), and their narrow boiling point difference can lead to separation problems. For example, separation by distillation can be both energy and cost intensive when using low temperature (cryogenic) and high pressure processes.[1] As a result, alternative strategies to separate olefin/paraffin mixtures that would result in capital and energy savings are of great interest. Eldridge[1] reviewed several recent technologies and efforts used to improve the separation of such mixtures. Of these, physical and chemical adsorption/absorption, advanced filtration, membranes, and extractive distillation offer the largest potential for energy and cost savings. However, to our knowledge, none have resulted in a commercially viable alternative to traditional distillation due to inherent problems associated with such systems. However, as energy costs rise, the efficient extraction of olefins continues to be of great academic and commercial interest.

Recently, considerable attention has been given to ionic liquids (ILs) as potential alternatives to common organic solvents in extraction processes. The nature and advantages of ILs are well documented, and they are considered to have substantial potential for use in green separation processes due to their admirable properties (such as stability, low flammability, and low volatility). The application of ILs in the separation of organic compounds in various product streams has also been explored extensively.[2−5] In a study by McFarlane et al., the separation of organic compounds from water as a contaminant was investigated using a variety of imidazolium, pyrrolidinium, and phosphonium-based hydrophobic ILs.[6] Hu et al. investigated the separation of ethyl acetate and ethanol using ILs with the tetrafluoroborate anion, further demonstrating the effectiveness of ILs in liquid−liquid extraction (LLE) processes.[7]

Enhancing the separation of ethylene from ethane using metal complexes/ILs has also been investigated. In the work of Galan Sanchez et al., the olefin/paraffin selectivity at a pressure of 1 bar was ∼30−50 times higher when using silver-based room temperature ILs when compared to standard ionic liquids.[8] Other promising alternatives have also evolved from the use olefin−metal complexes dissolved in an IL or by using complexing agents which form part of the IL itself. The underlying principle relies on the ability of certain ions such as silver or copper to react reversibly with olefins through π-complexation.[9−11] Among the transition metal ions, silver has a number of advantages and has been utilized in separation

Received: May 28, 2014
Accepted: October 31, 2014
Published: November 15, 2014

processes based on membrane separation,[12−14] chemical adsorption,[15,16] extractive distillation,[17] and extraction.[18−20] The chemical characteristics of silver impart its ability to bind to the olefins, whereas paraffins are unable to form such complexes. This reversible and specific interaction with olefins allows silver to act as an effective carrier for the olefin, as in the previously mentioned membrane transport process.

For the design of IL-based separation processes, both the cation and anion can be modified according to separation targets. Hence, ILs can be designed to control and modify the interaction between the silver cation (Ag^+) and its counteranion (X^-) in an IL/AgX system, affording enhanced silver cation chemical activity toward forming silver-olefin complexes.[21] Kang et al., for example, used composite IL/$AgNO_3$/polymer membranes for facilitated olefin transport (propylene/propane separation), and demonstrated improved interactions within the IL, silver nitrate, and poly(2-ethyl-2-oxazoline) system.[22] Although such strategies have been initiated, they currently remain unoptimized, giving considerable scope for future exploitation.

In our previous work, we investigated the ability of the silver bis(trifluoromethylsulfonyl)imide salt to entrain C5−C8 olefin/paraffin mixtures.[23] Here, we extend this work and describe an investigation into the extraction of linear α-olefins from paraffins with carbon numbers ranging from C5 to C8 using silver(I)/*N*,*N*-dimethylbenzamide bis(trifluoromethylsulfonyl)imide ([Ag(DMBA)$_2$][Tf$_2$N]) and silver(I)/propylamine bis(trifluoromethylsulfonyl)imide ([Ag(PrNH$_2$)$_2$][Tf$_2$N]) as the extractants. The solubilities of olefins and paraffins in these two ILs were determined, and their physical properties (density and viscosity) were measured and correlated to obtain direct information required to further develop chemical engineering extraction model using Aspen, for example. From preliminary testing using equimolar olefin/paraffin mixtures, the best-performing IL was selected for further detailed study, including an assessment of the impact of water. The universal quasi-chemical activity coefficient (UNIQUAC) model was then used to correlate the olefin/paraffin/IL phase equilibrium data and the quaternary phase equilibrium (olefin/paraffin/IL/water). COSMOthermX calculations were performed in order to provide some of the data required for the UNIQUAC model.

2. EXPERIMENTAL AND THEORETICAL METHODS

2.1. Chemicals and Characterizations. The mass fraction purities of all chemicals used are provided in Table S1 of the Supporting Information. All reagents were used without further purification. An ion exchange method was used to obtain the silver complexes. Silver nitrate (Ag[NO_3]) and lithium bis(trifluoromethylsulfonyl)imide (Li[Tf$_2$N]) salt solutions (5 M in deionized water, 18 MΩ) were prepared separately in ice baths at 0 °C. The ligand *N*,*N*-dimethylbenzamide (DMBA) was dissolved in water in a ∼ 2.2:1 mol ratio to silver, and was added dropwise to the Ag[NO_3] solution. After stirring for at least 10 min at 0 °C, the aqueous Li[Tf$_2$N] solution was added dropwise to the Ag[NO_3]/DMBA mixture with continuous stirring. A clear biphasic solution formed after letting the turbid mixture settle for ∼10 min. The lower phase contained mainly [Ag(DMBA)$_2$][Tf$_2$N], which was separated and washed with deionized water three times. A similar procedure was used in the synthesis of [Ag(PrNH$_2$)$_2$][Tf$_2$N]), except that propylamine was added dropwise into the Ag[NO_3] aqueous solution directly without prior dissolution in water. The resulting ILs were analyzed by elemental analysis (PerkinElmer 2400 CHN Elemental Analyzer) and inductively coupled plasma−optical emission spectrometry (ICP-OES, Perkin−Elmer Optima 4300). The purities of the two ILs were estimated at 98 ± 2 %. Elemental analysis results are shown in Table S2 of the Supporting Information. ^{1}H, ^{13}C, and ^{19}F NMR (Bruker 300 Hz) were also used to confirm the structures of the ILs; results are also included in the Supporting Information.

Thermogravimetric analysis (TGA, TA Instruments Q5000) using a nonisothermal method was conducted to measure the decomposition temperatures of the silver complexes. Samples of [Ag(DMBA)$_2$][Tf$_2$N] and [Ag(PrNH$_2$)$_2$][Tf$_2$N] (0.1−0.2 mg) were placed in a platinum pan and heated at a constant rate (10 °C/min) from room temperature to 600 °C. The densities (DM40 Density Meter, Mettler Toledo) and viscosities (Bohlin Gemini Rheometer, Rotonetic Drive 2, Malvern Instruments) of the complexes were measured over ranges based on the stability data from the TGA analysis combined together with an analysis of the consistency of density and viscosity data as a function of temperature up to 363 K. Even if TGA measurements (see Figure S1 of the Supporting Information) show that selected ILs have a similar thermal stability, close to 373 K, the temperature dependences on the viscosity and density reveal that the [Ag(PrNH$_2$)$_2$][Tf$_2$N] seems to be unstable for temperature higher than 333 K. Based on this observation, the physical properties of the pure [Ag(DMBA)$_2$][Tf$_2$N] were investigated from room temperature to 363 K, whereas these properties were reported herein up to 333 K in the case of the [Ag(PrNH$_2$)$_2$][Tf$_2$N].Karl Fischer titration for water content was carried out on a GR Scientific Cou-Lo Compact titrator. Water content analyses of the freshly prepared [Ag(DMBA)$_2$][Tf$_2$N] and [Ag(PrNH$_2$)$_2$][Tf$_2$N] were conducted three times, with water contents averaging 0.147 and 0.114 w/w%, respectively.

2.2. Solubility and Extraction Methods. The solubilities of the olefins and paraffins in the ILs were determined by mixing the hydrocarbons in excess with the silver complexes and stirring for 30 min at atmospheric pressure and 293 K. The water bath temperature was controlled to within ± 0.1 K, as measured by a standard Pt 100 Ω resistance thermometer. The complex, saturated by the olefin or paraffin, was allowed to settle for at least 60 min. The resulting IL-rich phase was separated and analyzed by ^{1}H NMR using deuterated dimethyl sulfoxide (DMSO-d_6) capillary tubes. For the extraction experiments, an equimolar mixture of the olefin/*n*-paraffin with the same carbon number was added to [Ag(DMBA)$_2$][Tf$_2$N] or [Ag(PrNH$_2$)$_2$][Tf$_2$N] in a volume ratio of 10:1 olefin/paraffin mixture:IL (e.g., 1.5 mL of IL, 15 mL of olefin/paraffin mixture). Phase equilibrium measurements were performed by stirring the ternary mixtures for 10 min at 293 K and atmospheric pressure in a water bath. The mixtures were left to settle for at least 60 min to reach phase equilibrium. Equilibration conditions (shorter stirring times (<60 min) and longer settling times) were examined by ^{1}H NMR to ensure that equilibrium had been achieved.

The IL with the better separation performance ([Ag(DMBA)$_2$][Tf$_2$N]) was selected for further study. Its extraction performance was assessed in the manner described above using olefin/paraffin mixtures prepared in 0.5:9.5, 1:9, 2:8, 8:2, 9:1, and 9.5:0.5 mol ratios. Samples of the lower (extracted) and upper phases (raffinate) were analyzed by ^{1}H NMR. Solubility and phase equilibrium data were obtained by integration of the characteristic peak of each species. The error in the NMR

dx.doi.org/10.1021/je5004669 | J. Chem. Eng. Data 2015, 60, 28−36

analysis using DMSO-d_6 capillary tubes was approximately ± 0.02 mole fraction. The absence of silver in the raffinate phase was confirmed by metal analysis using ICP. Furthermore, during this work the formation of Ag nanoparticle was not observed, even if it is very well-known that Ag^+ can be easily converted into Ag nanoparticles, which can result in the deterioration of separation performance and the long-term stability of selected extractants.[24−26]

The effect of water was studied by adding small amounts of water into the IL−organic hydrocarbon system. Using the same settling time, equilibrium was again reached. The equilibrium phase composition was obtained by ^{1}H NMR with observation of the water peak near 3.4 ppm. The accuracy of the measurement was ensured by Karl Fischer titration of the pure IL with low water content. The water content in the organic phase, also tested by Karl Fischer titration, proved to be lower than 0.2 mol %. Given this low value, subsequent calculations on the raffinate phase were performed on a water-free basis.

The LLE separation performance was evaluated based on the distribution coefficient β (eq 1) and the selectivity S (eq 2), which can be expressed as follows:

$$\beta = \frac{x_1^{\mathrm{E}}}{x_1^{\mathrm{R}}} \tag{1}$$

$$S = \frac{x_1^{\mathrm{E}}}{x_1^{\mathrm{R}}} / \frac{x_2^{\mathrm{E}}}{x_2^{\mathrm{R}}} \tag{2}$$

where x is the mole fraction of the component in each phase; the superscripts E and R denote the extract and raffinate phases, respectively; and the subscripts 1 and 2 denote the olefin and paraffin, respectively. Among the total number of solubility and phase equilibrium experiments, 18 groups were repeated to determine the combined statistical error, which was estimated as ∼ 5 % as a result of ^{1}H NMR analysis of the multiple repeats.

2.3. Modeling. The UNIQUAC model has been widely used for IL liquid−liquid phase equilibria since its introduction in 1975.[2,27−36] The model generally can be expressed as a mixture of two contributions to the activity coefficient γ_i of a species i via eq 3:

$$\ln \gamma_i = \ln \gamma_i^{\mathrm{C}} + \ln \gamma_i^{\mathrm{R}} \tag{3}$$

The term $\ln \gamma_i^{\mathrm{C}}$ represents the contributions of the molecular volume and surface area attributes of the compounds to the activity coefficient, as determined using the following eq 4:

$$\ln \gamma_i^{\mathrm{C}} = \ln \frac{\Theta_i}{x_i} + 5q_i \ln \frac{\Theta_i}{\Phi_i} + l_i - \frac{\Phi_i}{x_i} \sum_j x_j l_j \tag{4}$$

where Φ_i and Θ_i represent the normalized volume and surface area fraction of species i in the mixture, and x_i denotes its mole fraction. These parameters are determined by the volume r_i and surface area q_i using the eqs 5−7 below:

$$\Phi_i = \frac{x_i r_i}{\sum_j r_j x_j} \tag{5}$$

$$\Theta_i = \frac{x_i q_i}{\sum_j q_j x_j} \tag{6}$$

$$l_i = 5(r_i - q_i) - (r_i - 1) \tag{7}$$

The residual contribution $\ln \gamma_i^{\mathrm{R}}$ represents the interactions between the different compounds in the mixture and is defined by eq 8:

$$\ln \gamma_i^{\mathrm{R}} = q_i \left[1 - \ln\left(\sum_j \Theta_j \tau_{ji}\right) - \sum_j \frac{\Theta_j \tau_{ij}}{\sum_k \Theta_k \tau_{kj}} \right] \tag{8}$$

The interaction parameter τ_{ij} is defined by the interaction energy parameter a_{ij} for the interaction of species i and j as shown in eq 9:

$$\ln \tau_{ij} = -\frac{a_{ij}}{RT} \tag{9}$$

The symbols R and T are the ideal gas constant and temperature. Based on the equations described above, the Rachford−Rice flash calculation was applied to correlate the experimental data, i.e., to generate the tie lines of the liquid−liquid phase equilibria, by using the Microsoft Excel Solver software. A least-squares minimization approach was used iteratively to minimize the errors and obtain the optimized a_{ij} values. The root-mean-square deviation (rmsd; eq 10) was used to estimate the quality of the correlation:

$$\mathrm{rmsd} = \left\{ \sum_i \sum_j \sum_k (x_{ijk}^{\mathrm{exp}} - x_{ijk}^{\mathrm{calc}})^2 / 6n \right\}^{1/2} \tag{10}$$

where x is the mole fraction and the subscripts i, j, and k represent each component, phase, and the tie lines, respectively. The value n denotes the number of tie lines. In order to apply the UNIQUAC model to predict the solubility results ternary phase diagrams, r_i and q_i of the target molecules play important roles. Therefore, molecular structure calculations which included the van der Waals volumes and surface areas were performed using TURBOMOLE and COSMOthermX (version C30_1301, release 01.13, COSMOlogic). The structures were optimized with a convergence criterion of 10^{-8} Hartree in the gas phase. The TURBOMOLE 6.0 program package was used for all the density functional theory (DFT) calculations using the Resolution of Identity (RI) approximation.[37] The B3LYP functional was chosen for geometry optimization.[9,21,22,38−40] All the calculations were finished with the def-TZVP basis set, combining the RI technique calculations.[41,42] The $[Ag(DMBA)_2]^+$ and $[Ag(PrNH_2)_2]^+$ cations were each optimized independently of the $[Tf_2N]^-$ anion. Conformers of the cations were also considered in order to obtain accurate COSMO volume or surface area predictions. The anion used was directly extracted from the COSMOthermX database.

The structural properties of isolated clusters consisting of $[Ag(DMBA)_2][Tf_2N]$ and 1-pentene, *n*-pentane,1-hexene, *n*-hexane, 1-heptene, *n*-heptane, 1-octene, and *n*-octane were obtained by DFT calculations.

Once the molecular structures were optimized, the output COSMO files generated by TURBOMOLE were used with COSMOthermX to generate the COSMO volumes and surface areas. The van der Waals volumes and surface areas were then approximated by the following eqs 11 and 12, which can be found in the COSMOthermX manual:

$$r_i = \mathrm{V}_i^{\mathrm{COSMO}}/30 \tag{11}$$

$$q_i = \mathrm{A}_i^{\mathrm{COSMO}}/40 \tag{12}$$

where r_i and q_i are the van der Waals volumes and surface areas, respectively, and $\mathrm{V}_i^{\mathrm{COSMO}}$ and $\mathrm{A}_i^{\mathrm{COSMO}}$ are the COSMO

dx.doi.org/10.1021/je5004669 | J. Chem. Eng. Data 2015, 60, 28−36

volumes and surface areas generated by COSMOthermX. As stated, a Rachford-Rice flash calculation procedure was then used to estimate the solubility and tie lines from the resulting activity coefficients.

Based on molecular volume, Preiss et al. introduced in silico predictions of temperature-dependent densities of ILs in 2009.[43] Moreover, in 2010, Eiden et al. introduced a new method for in silico predictions of temperature-dependent viscosity and conductivity using molecular volume as an important known factor.[44] Since molecular volumes are basic values generated by COSMOthermX, these empirical models are embedded in the program to predict a series of temperature-dependent physical properties. Herein, we utilized this function of COSMOthermX to predict density and viscosity without revising any parameters. The temperature-dependence ranges were (273−415) K for the density predictions and (253−373) K for the viscosity predictions.

For the density measurements, the mean error (err_{ϕ}; eq 13) was defined as

$$err_{\phi} = \frac{\sum_i \left| \frac{x_i}{y_i} - 1 \right|}{N} \times 100\% \quad (13)$$

Here x denotes the calculated value and y denotes the independent observed value, with N being the sample size.

As viscosity predictions have wide error ranges in the literature,[44] the root-mean-square-error (rmse; eq 14) has been recommended for their estimation as follows:

$$\text{rmse} = \sqrt{\frac{\sum (x_{exp} - x_{calc})^2}{N}} \quad (14)$$

Here x is the decadal logarithm of the viscosity experimental value and N is the sample size.

3. RESULTS AND DISCUSSION

Before testing the extraction process, the densities (ρ, g·mL^{-1}) and viscosities (η, mPa·s) versus temperature were measured for $[Ag(DMBA)_2][Tf_2N]$ and $[Ag(PrNH_2)_2][Tf_2N]$ (Figures 1 and 2, respectively) in order to collect direct exploitable

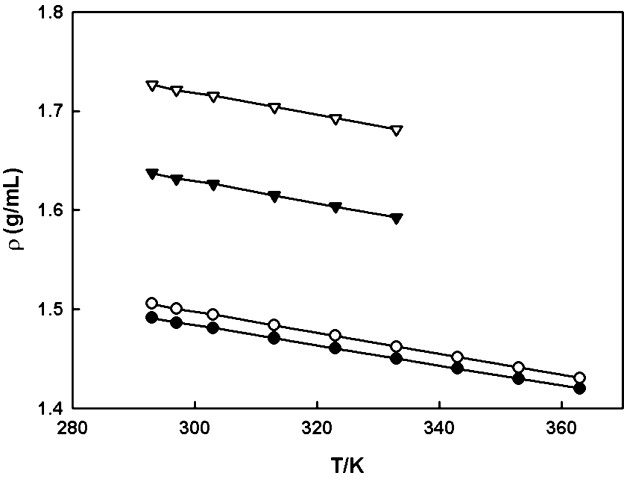

Figure 1. Temperature-dependent density measurements and predictions for $[Ag(DMBA)_2][Tf_2N]$: (●) experimental and (○) COSMOthermX prediction; and $[Ag(PrNH_2)_2][Tf_2N]$: (▼) experimental and (▽) COSMOthermX prediction.

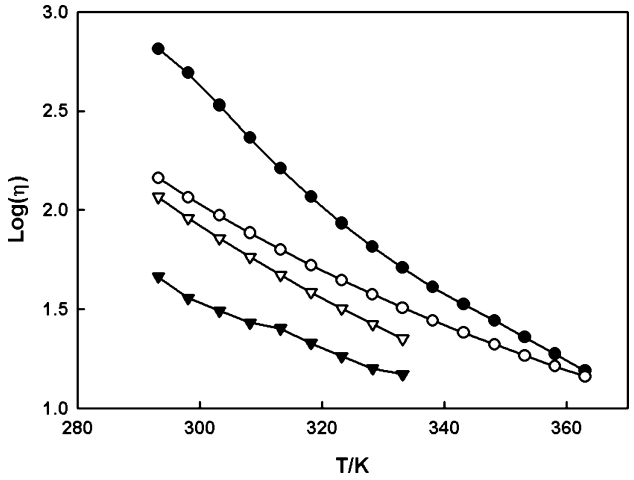

Figure 2. Temperature-dependent viscosity measurements and predictions for $[Ag(DMBA)_2][Tf_2N]$: (●) experimental and (○) COSMOthermX prediction; and $[Ag(PrNH_2)_2][Tf_2N]$: (▼) experimental and (▽) COSMOthermX prediction. All data were converted to the decadal logarithm scale.

information useful for the chemical engineering design of any process. The IL complexes synthesized within showed similar densities and viscosities to those previously reported; $[Ag(DMBA)_2][Tf_2N]$ (ρ = 1.47 g·mL^{-1}, η = 625.1 mPa·s) and $[Ag(PrNH_2)_2][Tf_2N]$ (ρ = 1.63 g·mL^{-1}, η = 36.52 mPa·s) at 296 K.[45] An analysis of TGA data (see Figure S1 of the Supporting Information) along with density and viscosity temperature dependences for formed complexes drives the upper limits for these determinations as 363 K for $[Ag(DMBA)_2][Tf_2N]$ and 333 K for $[Ag(PrNH_2)_2][Tf_2N]$. The mean errors calculated for the $[Ag(DMBA)_2][Tf_2N]$ and $[Ag(PrNH_2)_2][Tf_2N]$ density measurement predictions were (0.86 and 5.51) %, respectively, which are consistent with the relevant literature.[45] The rmse values for the $[Ag(DMBA)_2][Tf_2N]$ and $[Ag(PrNH_2)_2][Tf_2N]$ temperature-dependent viscosity measurements were 0.356 and 0.307, respectively. As can be seen from the plots of measured and predicted viscosities, at high temperature, the viscosity predictions tend to show improved accuracy. An analysis of predicted density and viscosity data clearly highlights that the COSMO-RS method cannot predict accurately the ion−ion and ion−amine type interactions in the case of the pure $[Ag(PrNH_2)_2][Tf_2N]$ as the predicted data sets are both overestimated. In this particular case, COSMO-RS suggests stronger interactions, which increase in fact the packing of compounds in solution driven by the presence of strong hydrogen bonding, resulting in a higher density and viscosity of the solution than those observed experimentally.

Preliminary experiments were carried out to determine which IL was more efficient for olefin/paraffin separation at 293 K. Compared with other similar extraction experiments,[18,20] our systems appeared to reach equilibrium faster. Table 1 illustrates the solubility ratios of the hydrocarbon components, and the selectivity and distribution coefficients with respect to equimolar olefin/paraffin feed compositions for both silver complexes. Clearly, a large difference between the two ILs can be observed. The solubility mole ratios of olefins in $[Ag(DMBA)_2][Tf_2N]$ range from 1.47 to 2.23, which are significantly higher than those in $[Ag(PrNH_2)_2][Tf_2N]$ (0.49 to 0.66). As discussed earlier, the olefin can form complexes with

dx.doi.org/10.1021/je5004669 | J. Chem. Eng. Data 2015, 60, 28−36

Table 1. Olefin and Paraffin Solubility in Neat IL Expressed in Mol Ratio between Olefin or Paraffin and IL at 293 K and 0.1 MPa[a]

		C5	C6	C7	C8
olefin solubility	$[Ag(DMBA)_2][Tf_2N]$	2.23	2.11	1.57	1.47
	$[Ag(PrNH_2)_2][Tf_2N]$	0.74	0.71	0.67	0.49
paraffin solubility	$[Ag(DMBA)_2][Tf_2N]$	0.17	0.14	0.10	0.06
	$[Ag(PrNH_2)_2][Tf_2N]$	0.36	0.32	0.19	0.17
selectivity, S	$[Ag(DMBA)_2][Tf_2N]$	4.43	4.38	5.43	4.66
	$[Ag(PrNH_2)_2][Tf_2N]$	1.15	1.10	1.38	1.45
distribution coefficient, β	$[Ag(DMBA)_2][Tf_2N]$	0.92	0.95	0.86	0.85
	$[Ag(PrNH_2)_2][Tf_2N]$	0.58	0.36	0.33	0.30

[a]The selectivity and distribution coefficient were calculated based on an (olefin + paraffin + IL) ternary mixture, containing an (olefin + paraffin): IL volume ratio close to 10:1 while the olefin: paraffin mol ratio was set to 1 at 293 K and 0.1 MPa. $u(n_i)$ = 0.005 mol with i = olefin, paraffin or IL; $u(T)$ = 0.1 K.

Ag^+, and therefore, the interactions between the IL and olefin are dominated by coordination instead of van der Waals forces when establishing liquid−liquid equilibrium. The olefin solubility results here suggest a greater extent of olefin−Ag^+ complexation in $[Ag(DMBA)_2][Tf_2N]$ than in $[Ag(PrNH_2)_2][Tf_2N]$. This implies that the binding constant between propylamine and silver is stronger than that with DMBA. This is in agreement with Dai et al., in which authors quantified in detail the stoichiometry of formed complexes in solution using similar composition and IL structure.[45] Clearly, a weaker complexation between the silver and the ligand would enhance performance for olefin/paraffin extraction by allowing the silver to coordinate to the olefin more easily. With regard to the paraffins, their solubilities in $[Ag(PrNH_2)_2][Tf_2N]$ are more than twice those in $[Ag(DMBA)_2][Tf_2N]$. This can be explained by the molecular interactions between the paraffins and ligands. Structurally, the propylamine ligand bears an alkyl chain whereas DMBA is a phenyl group-based amide. On the basis of the "like dissolves like" principle, the propylamine-based IL would be expected to be more paraffin soluble. As both higher olefin and lower paraffin solubilities in the IL lead to better separation selectivity, we can conclude that $[Ag(DMBA)_2][Tf_2N]$ is a better partitioning candidate. This is supported by the selectivity and distribution coefficient results listed in Table 1. The selectivity of $[Ag(DMBA)_2][Tf_2N]$ ranges from 4.43 to 5.43, compared with 1.1 to 1.44 for the other complex. Also, $[Ag(DMBA)_2][Tf_2N]$ exhibited a higher distribution coefficient, which is believed to be mainly due a larger amount of olefin−silver complexation in this IL.

The influence of chain length was also studied; both ILs showed declining olefin selectivity when the carbon number decreased. Paraffin solubility also showed a declining trend with increasing carbon number. This phenomenon suggests that interactions between the IL and the olefin or paraffin weaken when the alkane chain length increases. The S values, however, appeared to increase, whereas β decreased with increasing alkane chain. This decreased β is consistent with the decreased solubility of the olefin in the extract phase.

A detailed study of phase equilibria was carried out on $[Ag(DMBA)_2][Tf_2N]$ as it showed better separation performance. Figure 3 shows the ternary phase diagrams for olefin/paraffin mixtures of different carbon numbers. As discussed previously, the water content was low in this system (i.e., less than 0.2 mol %), and therefore under these conditions the data is plotted on a water-free basis. According to the separation

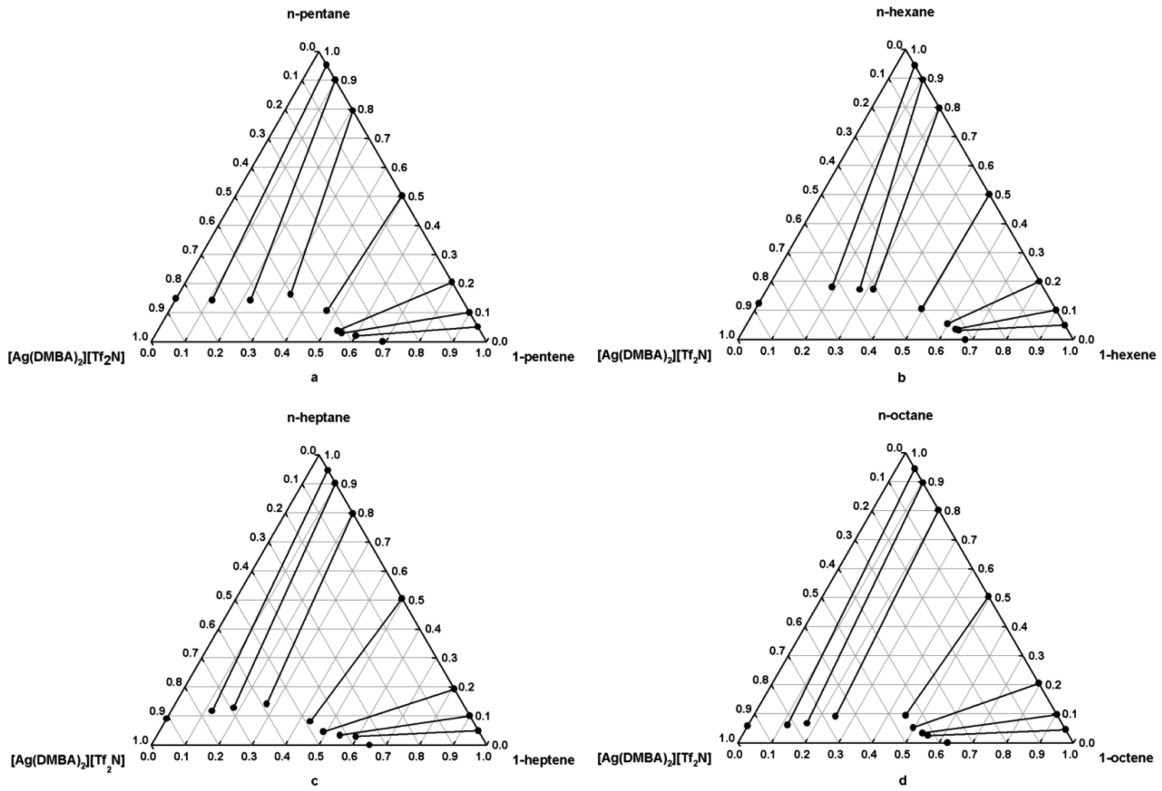

Figure 3. Experimental liquid−liquid equilibrium systems at 293 K: (a) {1-pentene + *n*-pentane + $[Ag(DMBA)_2][Tf_2N]$}; (b) [{1-hexene + *n*-hexane + $[Ag(DMBA)_2][Tf_2N]$}; (c) {1-heptene + *n*-heptane + $[Ag(DMBA)_2][Tf_2N]$}; and (d) [{1-octene + *n*-octane + $[Ag(DMBA)_2][Tf_2N]$}.

dx.doi.org/10.1021/je5004669 | J. Chem. Eng. Data 2015, 60, 28−36

performance plots of Figure 4, the highest S and β were 33 and 2.3 for the C8 and C7 systems, respectively. The selectivity and

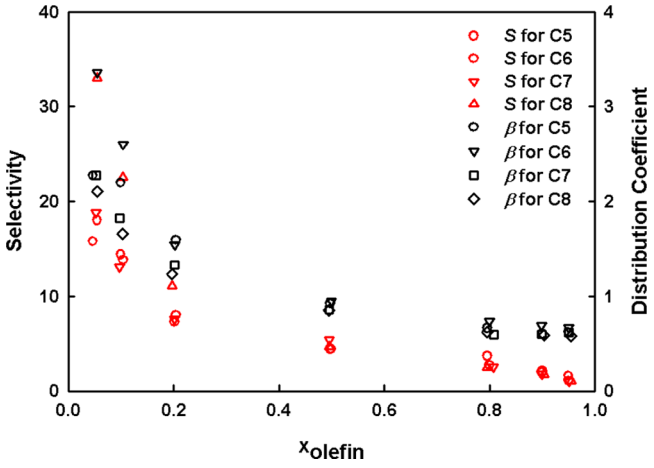

Figure 4. Selectivity and distribution coefficient as a function of mole fraction of olefin in raffinate phase using $[Ag(DMBA)_2][Tf_2N]$ as extractant at 293 K.

distribution coefficients decreased with an increasing olefin composition in the raffinate phase. Generally, the separation performance was better for the longer chain olefin/paraffin separation systems. The results reported here are significantly better than those previously reported. For example, $[C_4mim][Tf_2N]/Ag[Tf_2N]$ only showed a maximum S of 15 versus 18 using $[Ag(DMBA)_2][Tf_2N]$ albeit for hexane/hexane separation.[18] In addition, the use of the amine-based ligands to stabilize the $AgTf_2N$−olefin complex resulted in higher S and β values compared to analogous experiments conducted in the absence of the amines.[23]

The impact of water as an impurity was next studied. Figure 5 shows the solubilities of the olefins and paraffins with respect to the water/Ag ratio. Solubility tests of the olefins in $[Ag(DMBA)_2][Tf_2N]$ were initially conducted with different concentrations of added water. The olefin solubility decreased slightly as the water content increased, which was expected as the olefins are hydrophobic. However, the paraffin solubility

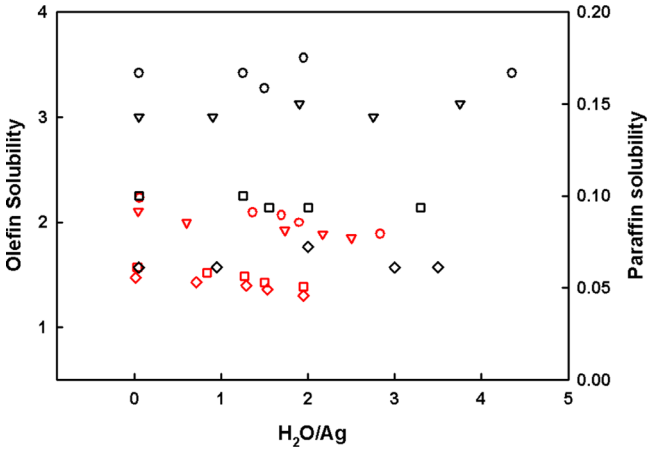

Figure 5. Olefin (red symbols) and paraffin (black symbols) solubilities in the $[Ag(DMBA)_2][Tf_2N]$ extractant as a function of the H_2O/Ag^+ mole ratio at 293 K. C5−C8 compounds are indicated by the circle, triangle, rectangle, and rhombus symbols, respectively.

remained nearly constant except for small fluctuations within the range of experimental error. Figure 6 illustrates selectivities

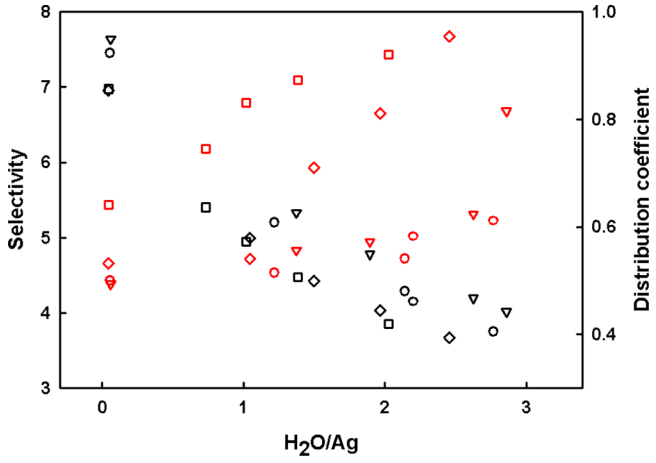

Figure 6. Selectivities and distribution coefficients as functions of the H_2O/Ag mole ratio using $[Ag(DMBA)_2][Tf_2N]$ as extractant with 1:1 olefin/paraffin feed compositions at 293 K. Olefin values are indicated in red and those for the paraffins are shown in black. C5−C8 compounds are indicated by the circle, triangle, rectangle, and rhombus symbols, respectively.

and distribution coefficients with the variation of the water/Ag ratio. S increased while β decreased when water was added to the equimolar feed. Thus, water improved the selectivity by aiding the partition of species to the raffinate phase. Figure 7 gives a comparison between phase separations at low and high water contents. The tie lines were extended slightly due to the reduced partitioning of both the olefins and paraffins. In the presence of a high water content, the highest S value was enhanced to about 38 in the1-octene/*n*-octane system. All experimental details can be found in the SI.

From the solubility and extraction experimental data, the UNIQUAC model was applied to the $[Ag(DMBA)_2][Tf_2N]$ system. V_i^{COSMO}, A_i^{COSMO}, and the optimized a_{ij} values are given in Table 2. Using 108 groups of experimental data in total, the calculated rmsds are (1.37, 0.86, 0.75, and 1.48) % for the C5−C8 systems, respectively. Detailed correlation results are provided in the SI. Such metal-containing IL LLE-system data correlations using UNIQUAC have been rarely attempted, and hence, these results exemplify and confirm the wide and practical utility of this model.

4. CONCLUSION

From the temperature-dependent density and viscosity studies, COSMOthermX was able to provide density predictions within a satisfactory error range. However, relatively low accuracy was found for the prediction of viscosity. The viscosity and density data can provide information for the design of extraction and extractive distillation systems as well as other potential chemical engineering applications. For the purpose of separating olefins from olefin/paraffin mixtures, the liquid−liquid equilibria for olefin, paraffin, and $[Ag(DMBA)_2][Tf_2N]$ or $[Ag(PrNH_2)_2][Tf_2N]$ were determined at T = 293 K and atmospheric pressure. Based on olefin solubility testing, we conclude that DMBA interacts more weakly with the silver ion than propylamine. From the extraction LLE data, $[Ag(DMBA)_2][Tf_2N]$ was found to be a better extracting agent for the separation because of its high selectivity and distribution

dx.doi.org/10.1021/je5004669 | J. Chem. Eng. Data 2015, 60, 28−36

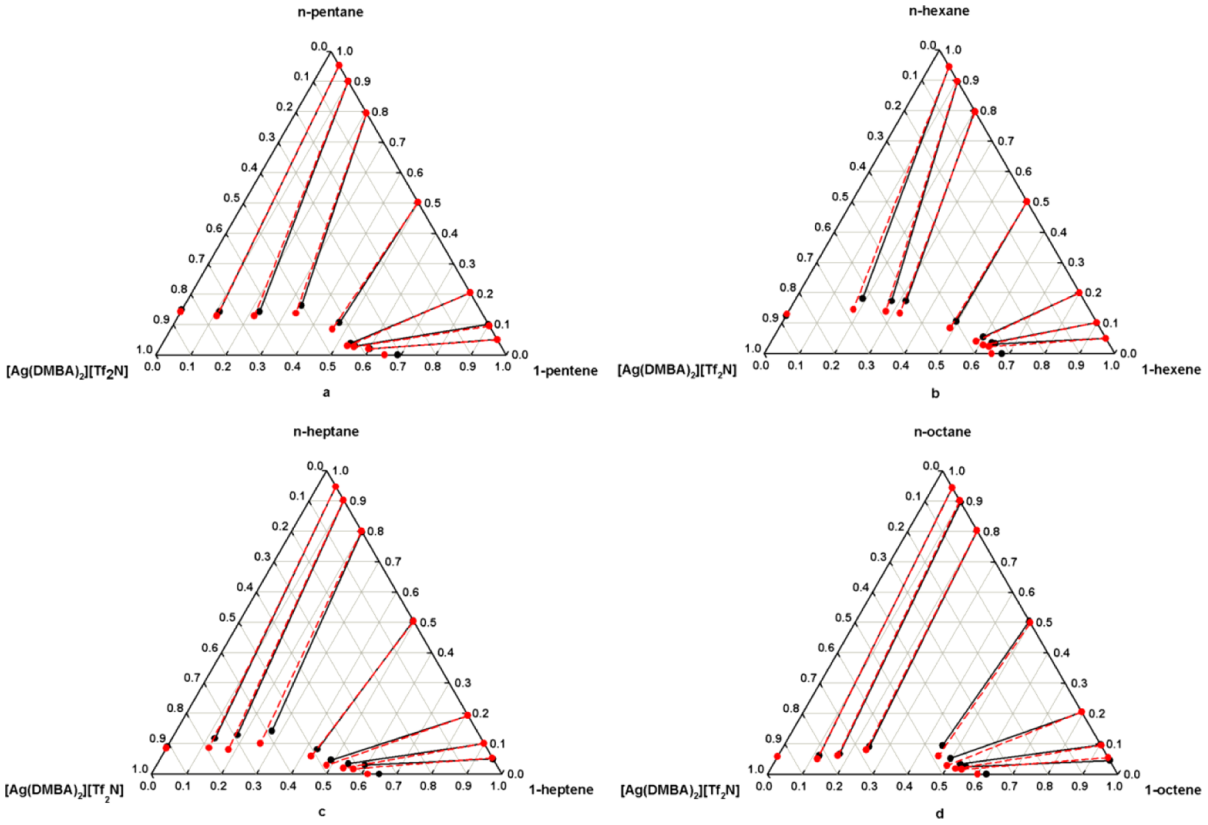

Figure 7. Experimental liquid−liquid equilibrium systems at 293 K in the presence of water (black dots: low water content; red dots: high water content). (a) {1-pentene + *n*-pentane + $[Ag(DMBA)_2][Tf_2N]$}; (b) [{1-hexene + *n*-hexane + $[Ag(DMBA)_2][Tf_2N]$}; (c) {1-heptene + *n*-heptane + $[Ag(DMBA)_2][Tf_2N]$}; and (d) [{1-octene + *n*-octane + $[Ag(DMBA)_2][Tf_2N]$}.

Table 2. Surface Area *r*, Volume *q*, and Binary Interaction Energy Parameters a_{ij} for the UNIQUAC Model

			binary interaction energy parameters									
r	*q*		$[Ag(DMBA)_2][Tf_2N]$	*n*-pentane	1-pentene	*n*-hexane	1-hexene	*n*-heptane	1-heptene	*n*-octane	1-octene	H_2O
19.87	16.30	$[Ag(DMBA)_2][Tf_2N]$	0.00	−2308.70	29.60	−185.90	−48.51	−238.67	32.70	−165.73	−55.26	−196.62
0.92	1.40	H_2O	−294.50	0.00	382.03	88.93	823.58	117.23	140.24	−91.10	88.32	−97.63
3.83	3.32	*n*-pentane	592.90	1005.56	0.00	−77.09	NA	NA	NA	NA	NA	NA
3.60	3.10	1-pentene	687.90	494.61	214.49	0.00	NA	NA	NA	NA	NA	NA
4.50	3.86	*n*-hexane	516.23	1376.04	NA	NA	0.00	418.96	NA	NA	NA	NA
4.27	3.64	1-hexene	968.25	446.20	NA	NA	−181.66	0.00	NA	NA	NA	NA
5.17	4.40	*n*-heptane	211.48	2261.40	NA	NA	NA	NA	0.00	53.73	NA	NA
4.94	4.18	1-heptene	438.12	810.87	NA	NA	NA	NA	24.44	0.00	NA	NA
5.85	4.94	*n*-octane	504.88	1229.46	NA	NA	NA	NA	NA	NA	0.00	81.65
5.62	4.72	1-octene	546.92	761.90	NA	NA	NA	NA	NA	NA	29.77	0.00

coefficient. The selectivities for 1-heptene and 1-octene were higher than those for 1-pentene and 1-hexene. Water as an impurity in the system had a positive effect in terms of the selectivity and a negative impact on the distribution coefficient. Furthermore, the good correlation between the experimental solubility and extraction data and the UNIQUAC model will facilitate further study on the screening of ionic liquids in olefin/paraffin separations.

■ ASSOCIATED CONTENT

Supporting Information

Purity and source of each starting material are reported in Table S1. Results of elemental analysis performed for selected ionic liquids are provided in Table S2, while their ^1H, ^{13}C, and ^{19}F NMR spectra are shown in Figures S2−S7. Measured density and viscosity for each ionic liquid are reported in Table S3. DSC thermograms of pure ionic liquids are reported in Figure S1. The composition of each phase for investigated mixtures is listed in Tables S4 and S5. Comparisons between UNIQUAC calculations with experimental LLE data are shown in Table S6. This material is available free of charge via the Internet at http://pubs.acs.org.

■ AUTHOR INFORMATION

Corresponding Author

*Address: CENG, FIChemE Director, Qatar University Honor's Program, Dept. of Chemical Engineering, Corr 1, Male campus, B05, Room 104, P.O. Box 2713, Doha, Qatar.

Tel: (974) 4403−4993/4990. Fax: (974) 4403-4001. E-mail: m.khraisheh@qu.edu.qa.

Funding

The authors would like to thank the Qatar National Priorities Research Program (NPRP) Foundation under program NPRP 09-739-2-284 for its support of this work.

Notes

The authors declare no competing financial interest.

LIST OF ABBREVIATIONS:

a, interaction energy parameter
A_i^{COSMO}, calculated surface area
β, distribution coefficient
DFT, density functional theory
DMBA, *N*,*N*-dimethylbenzamide
E, extract phase
η, viscosity
err_ϕ, mean error
γ_i, activity coefficient
IL, ionic liquid
LLE, liquid−liquid extraction
Φ_i, normalized volume
q_i, surface area
R, raffinate phase
R, ideal gas constant
ρ, density
r_i, volume
RI, resolution of identity
rmsd, root-mean-square deviation
rmse, root-mean-square error
S, selectivity
T, temperature
τ, interaction parameter
Θ_i, surface area fraction
UNIQUAC, universal quasichemical activity coefficient model
V_i^{COSMO}, calculated volume
x, mole fraction

REFERENCES

(1) Eldridge, R. B. Olefin Paraffin Separation Technology - a Review. *Ind. Eng. Chem. Res.* **1993**, *10*, 2208−2212.
(2) Al-Jimaz, A. S.; Alkhaldi, K. H. A. E.; Al-Rashed, M. H.; Fandary, M. S.; AlTuwaim, M. S. Study on the Separation of Propylbenzene from Alkanes using Two Methylsulfate-Based Ionic Liquids at (313 and 333) K. *Fluid Phase Equilib.* **2013**, *354*, 29−37.
(3) Zhou, T.; Wang, Z.; Chen, L.; Ye, Y.; Qi, Z.; Freund, H.; Sundmacher, K. Evaluation of the ionic liquids 1-alkyl-3-methylimidazolium hexafluorophosphate as a solvent for the extraction of benzene from cyclohexane: (Liquid+liquid) equilibria. *J. Chem. Thermodyn.* **2012**, *48*, 145−149.
(4) Vidal, L.; Parshintsev, J.; Hartonen, K.; Canals, A.; Riekkola, M.-L. Ionic Liquid-Functionalized Silica for Selective Solid-Phase Extraction of Organic Acids, Amines and Aldehydes. *J. Chromatogr. A* **2012**, *1226*, 2−10.
(5) Chen, D.-X.; OuYang, X.-K.; Wang, Y.-G.; Yang, L.-Y.; He, C.-H. Liquid−Liquid Extraction of Caprolactam from Water using Room Temperature Ionic Liquids. *Sep. Purif. Technol.* **2013**, *104*, 263−267.
(6) McFarlane, J.; Ridenour, W. B.; Luo, H.; Hunt, R. D.; DePaoli, D. W.; Ren, R. X. Room Temperature Ionic Liquids for Separating Organics from Produced Water. *Sep. Sci. Technol.* **2005**, *6*, 1245−1265.
(7) Hu, X.; Li, Y.; Cui, D.; Chen, B. Separation of Ethyl Acetate and Ethanol by Room Temperature Ionic Liquids with the Tetrafluoroborate Anion. *J. Chem. Eng. Data* **2008**, *2*, 427−433.
(8) Galán Sánchez, L. M.; Meindersma, G. W.; Haan, A. B. Potential of Silver-Based Room-Temperature Ionic Liquids for Ethylene/Ethane Separation. *Ind. Eng. Chem. Res.* **2009**, *23*, 10650−10656.
(9) Chen, J. P.; Yang, R. T. A Molecular-Orbital Study of the Selective Adsorption of Simple Hydrocarbon Molecules on Ag^+-Exchanged and Cu^+-Exchanged Resins and Cuprous Halides. *Langmuir* **1995**, *9*, 3450−3456.
(10) Hartley, F. R. Thermodynamic Data for Olefin and Acetylene Complexes of Transition-Metals. *Chem. Rev.* **1973**, *2*, 163−190.
(11) Kim, J. H.; Min, B. R.; Won, J.; Kang, Y. S. Complexation Mechanism of Olefin with Silver Ions Dissolved in A Polymer Matrix and its Effect on Facilitated Olefin Transport. *Chem.—Eur. J.* **2002**, *3*, 650−654.
(12) Faiz, R.; Li, K. Olefin/Paraffin Separation using Membrane based Facilitated Transport/Chemical Absorption Techniques. *Chem. Eng. Sci.* **2012**, *73*, 261−284.
(13) Ravanchi, M. T.; Kaghazchi, T.; Kargaric, A. Facilitated Transport Separation of Propylene-Propane: Experimental and Modeling Study. *Chem. Eng. Process.* **2010**, *3*, 235−244.
(14) Kim, J. H.; Min, B. R.; Won, J.; Kang, Y. S. Revelation of Facilitated Olefin Transport through Silver-Polymer Complex Membranes using Anion Complexation. *Macromolecules* **2003**, *12*, 4577−4581.
(15) Ortiz, A.; Galan, L. M.; Gorri, D.; de Haan, A. B.; Ortiz, I. Reactive Ionic Liquid Media for the Separation of Propylene/Propane Gaseous Mixtures. *Ind. Eng. Chem. Res.* **2010**, *16*, 7227−7233.
(16) van Miltenburg, A.; Zhu, W.; Kapteijn, F.; Moulijn, J. A. Adsorptive Separation of Light Olefin/Paraffin Mixtures. *Chem. Eng. Res. Des.* **2006**, *A5*, 350−354.
(17) Wentink, A. E.; Kuipers, N. J. M.; de Haan, A. B.; Scholtz, J.; Mulder, H. Olefin Isomer Separation By Reactive Extractive Distillation: Modelling of Vapour−Liquid Equilibria and Conceptual Design for 1-Hexene Purification. *Chem. Eng. Process.* **2007**, *9*, 800−809.
(18) Li, R. L.; Xing, H. B.; Yang, Q. W.; Zhao, X.; Su, B. G.; Bao, Z. B.; Yang, Y. W.; Ren, Q. L. Selective Extraction of 1-Hexene Against n-Hexane in Ionic Liquids with or without Silver Salt. *Ind. Eng. Chem. Res.* **2012**, *25*, 8588−8597.
(19) Lei, Z.; Arlt, W.; Wasserscheid, P. Selection of Entrainers in the 1-Hexene/n-Hexane System with A Limited Solubility. *Fluid Phase Equilib.* **2007**, *1*, 29−35.
(20) Lei, Z. G.; Arlt, W.; Wasserscheid, P. Separation of 1-Hexene and n-Hexane with Ionic Liquids. *Fluid Phase Equilib.* **2006**, *1−2*, 290−299.
(21) Won, J.; Kim, D. B.; Kang, Y. S.; Choi, D. K.; Kim, H. S.; Kim, C. K.; Kim, C. K. An ab initio Study of Ionic Liquid Silver Complexes as Carriers in Facilitated Olefin Transport Membranes. *J. Membr. Sci.* **2005**, *1−2*, 37−44.
(22) Kang, S. W.; Char, K.; Kim, J. H.; Kim, C. K.; Kang, Y. S. Control of Ionic Interactions in Silver Salt-Polymer Complexes with Ionic Liquids: Implications for Facilitated Olefin Transport. *Chem. Mater.* **2006**, *7*, 1789−1794.
(23) Wang, Y.; Thompson, J.; Zhou, J.; Goodrich, P.; Atilhan, M.; Pensado, A. S.; Kirchner, B.; Rooney, D.; Jacquemin, J.; Khraisheh, M. Use Of Water in Aiding Olefin/Paraffin (Liquid+Liquid) Extraction via Complexation with a Silver Bis(Trifluoromethylsulfonyl)Imide Salt. *J. Chem. Thermodyn.* **2014**, *77*, 230−240.
(24) Lee, D. H.; Kang, Y. S.; Kim, J. H. Olefin Separation Performances and Coordination Behaviors of Facilitated Transport Membranes Based on Poly(styrene-b-isoprene-b-styrene)/Silver Salt Complexes. *Macromol. Res.* **2009**, *2*, 104−109.
(25) Fallanza, M.; Ortiz, A.; Gorri, D.; Ortiz, I. Polymer−Ionic Liquid Composite Membranes for Propane/Propylene Separation by Facilitated Transport. *J. Membr. Sci.* **2013**, *444*, 164−172.
(26) Azhin, M.; Kaghazchi, T.; Rahmani, M. A Review on Olefin/Paraffin Separation using Reversible Chemical Complexation Technology. *J. Ind. Eng. Chem.* **2008**, *5*, 622−638.

(27) Abrams, D. S.; Prausnitz, J. M. Statistical Thermodynamics of Liquid Mixtures: A New Expression for the Excess Gibbs Energy of Partly or Completely Miscible Systems. *AIChE J.* **1975**, *1*, 116−128.
(28) Banerjee, T.; Singh, M. K.; Sahoo, R. K.; Khanna, A. Volume, Surface and UNIQUAC Interaction Parameters for Imidazolium Based Ionic Liquids via Polarizable Continuum Model. *Fluid Phase Equilib.* **2005**, *1*−*2*, 64−76.
(29) Gutierrez, J. P.; Meindersma, W.; de Haan, A. B. Binary and Ternary (Liquid + Liquid) Equilibrium for {Methylcyclohexane (1) + Toluene (2) + 1-Hexyl-3-Methylimidazolium Tetracyanoborate (3)/1-Butyl-3-Methylimidazolium Tetracyanoborate (3)}. *J. Chem. Thermodyn.* **2011**, *11*, 1672−1677.
(30) Haghtalab, A.; Paraj, A. Computation of Liquid−Liquid Equilibrium of Organic-Ionic Liquid Systems using NRTL, UNIQUAC and NRTL-NRF Models. *J. Mol. Liq.* **2012**, *171*, 43−49.
(31) Kato, R.; Gmehling, J. Measurement and Correlation of Vapor−Liquid Equilibria of Binary Systems containing the Ionic Liquids [EMIM][$(CF_3SO_2)_2N$], [BMIM][$(CF_3SO_2)_2N$], [MMIM]-[$(CH_3)_2PO_4$] and Oxygenated Organic Compounds Respectively Water. *Fluid Phase Equilib.* **2005**, *1*, 38−43.
(32) Królikowska, M.; Karpińska, M.; Zawadzki, M. Phase Equilibria Study of (Ionic Liquid + Water) Binary Mixtures. *Fluid Phase Equilib.* **2013**, *354*, 66−74.
(33) Rabari, D.; Banerjee, T. Biobutanol and n-Propanol Recovery using a Low Density Phosphonium Based Ionic Liquid at T = 298.15 K and p = 1 atm. *Fluid Phase Equilib.* **2013**, *355*, 26−33.
(34) Ravilla, U. K.; Banerjee, T. Liquid Liquid Equilibria of Imidazolium based Ionic Liquid + Pyridine + Hydrocarbon at 298.15 K: Experiments and Correlations. *Fluid Phase Equilib.* **2012**, *324*, 17−27.
(35) Shah, M. R.; Anantharaj, R.; Banerjee, T.; Yadav, G. D. Quaternary (Liquid + Liquid) Equilibria for Systems of Imidazolium based Ionic Liquid + Thiophene + Pyridine + Cyclohexane at 298.15 K: Experiments and Quantum Chemical Predictions. *J. Chem. Thermodyn.* **2013**, *62*, 142−150.
(36) Simoni, L. D.; Lin, Y.; Brennecke, J. F.; Stadtherr, M. A. Modeling Liquid−Liquid Equilibrium of Ionic Liquid Systems with NRTL, Electrolyte-NRTL, and UNIQUAC. *Ind. Eng. Chem. Res.* **2007**, *1*, 256−272.
(37) Weigend, F.; Häser, M. RI-MP2: First Derivatives and Global Consistency. *Theor. Chem. Acc.* **1997**, *1*−*4*, 331−340.
(38) Jiang, D. E.; Dai, S. First Principles Molecular Dynamics Simulation of a Task-Specific Ionic Liquid based on Silver-Olefin Complex: Atomistic Insights into a Separation Process. *J. Phys. Chem. B* **2008**, *33*, 10202−10206.
(39) Kim, C. K.; Kim, C. K.; Lee, B. S.; Won, J.; Kim, H. S.; Kang, Y. S. Density Functional Theory Studies on the Reaction Mechanisms of Silver Ions with Ethylene in Facilitated Transport Membranes: A Modeling Study. *J. Phys. Chem. A* **2001**, *39*, 9024−9028.
(40) Talaty, E. R.; Raja, S.; Storhaug, V. J.; Dölle, A.; Carper, W. R. Raman and Infrared Spectra and ab Initio Calculations of C_{2-4}MIM Imidazolium Hexafluorophosphate Ionic Liquids. *J. Phys. Chem. B* **2004**, *35*, 13177−13184.
(41) Schafer, A.; Huber, C.; Ahlrichs, R. Fully Optimized Contracted Gaussian Basis Sets of Triple Zeta Valence Quality for Atoms Li to Kr. *J. Chem. Phys.* **1994**, *8*, 5829−5835.
(42) Weigend, F.; Häser, M.; Patzelt, H.; Ahlrichs, R. RI-MP2: Optimized Auxiliary Basis Sets and Demonstration of Efficiency. *Chem. Phys. Lett.* **1998**, *1*−*3*, 143−152.
(43) Preiss, U. P. R. M.; Slattery, J. M.; Krossing, I. In Silico Prediction of Molecular Volumes, Heat Capacities, and Temperature-Dependent Densities of Ionic Liquids. *Ind. Engineer. Chem. Res.* **2009**, *4*, 2290−2296.
(44) Eiden, P.; Bulut, S.; Köchner, T.; Friedrich, C.; Schubert, T.; Krossing, I. In Silico Predictions of the Temperature-Dependent Viscosities and Electrical Conductivities of Functionalized and Nonfunctionalized Ionic Liquids. *J. Phys. Chem. B* **2010**, *2*, 300−309.
(45) Huang, J. F.; Luo, H. M.; Liang, C. D.; Jiang, D. E.; Dai, S. Advanced Liquid Membranes Based on Novel Ionic Liquids for Selective Separation of Olefin/Parafrin via Olefin-Facilitated Transport. *Ind. Eng. Chem. Res.* **2008**, *3*, 881−888.